# Lorentz Mapping of Magnetic Fields in Hot Dense Plasmas

R. D. Petrasso, C. K. Li, F. H. Seguin, J. R. Rygg,* and J. A. Frenje
*Plasma Science and Fusion Center, Massachusetts Institute of Technology, Cambridge, Massachusetts 02139, USA*

R. Betti, J. P. Knauer, and D. D. Meyerhofer
*Laboratory for Laser Energetics, University of Rochester, Rochester, New York 14623, USA*

P. A. Amendt, D. H. Froula, O. L. Landen, P. K. Patel, J. S. Ross, and R. P. J. Town
*Lawrence Livermore National Laboratory, Livermore, California 94551, USA*
(Received 12 March 2009; published 17 August 2009)

Unique detection of electromagnetic fields and identification of field type and strength as a function of position were used to determine the nature of self-generated fields in a novel experiment with laser-generated plasma bubbles on two sides of a plastic foil. Field-induced deflections of monoenergetic 15-MeV probe protons passing through the two bubbles, measured quantitatively with proton radiography, were combined with Lorentz mapping to provide separate measurements of magnetic and electric fields. The result was absolute identification and measurement of a toroidal magnetic field around each bubble and determination that any electric field component parallel to the foil was below measurement uncertainties.

DOI: 10.1103/PhysRevLett.103.085001 PACS numbers: 52.38.Fz, 52.50.Jm, 52.70.Nc

Spontaneous generation of magnetic ($\boldsymbol{B}$) fields occurs pervasively in galactic [1,2] and stellar [3] settings and in numerous laboratory plasma experiments [2,4]. For the case of the hot, dense plasmas of laser-plasma experiments [4,5], or for scaled astrophysics experiments in the laboratory [2,4], self-generated magnetic and electric fields are often intertwined and inextricably coupled to the dynamics of the plasma evolution. This coupling makes the field generation process complicated and also means that the effects of the fields can directly or indirectly act back on the plasma itself. Measuring local, self-generated fields, and distinguishing between electric ($\boldsymbol{E}$) and magnetic fields, is a formidable task [6].

In this Letter we describe a monoenergetic proton radiography method that, when used in combination with Lorentz force mapping, allows for precise measurement of plasma field strengths as well as unequivocal discrimination between electric and magnetic fields. Measurement of electromagnetic fields in a high-energy-density plasma can be made by passing monoenergetic protons through the plasma and observing how their trajectories are deflected by the fields. Any trajectory bending is due to the Lorentz force

$$\boldsymbol{F} = q\left(\boldsymbol{E} + \frac{\boldsymbol{v} \times \boldsymbol{B}}{c}\right), \tag{1}$$

where $q$ is the proton charge and $\boldsymbol{v}$ is the proton velocity, acting over a path length $\ell$ characteristic of the fields' spatial extent. For true quantitative analysis of data it is critical that $\boldsymbol{v}$ be known accurately. If it is known in advance whether a field is $\boldsymbol{B}$ or $\boldsymbol{E}$, Eq. (1) can be used directly to relate any observed trajectory bending to field strength. If there is bending observed but no absolute knowledge of which field is present, the individual contributions of $\boldsymbol{E}$ and $\boldsymbol{B}$ can be determined with two independent measurements. This discrimination can be accomplished by three methods, though practical implementation is often challenging. The first method involves measurements on the same plasma made in the same way but with the direction of $\boldsymbol{v}$ reversed; the second utilizes measurements made of the same plasma but with protons of two discrete values of $|\boldsymbol{v}|$ (as illustrated in Ref. [7]); and the third utilizes measurements on two plasmas that are identical except for the reversal of any $\boldsymbol{B}$ field.

The experiment reported here utilized the third method to resolve ambiguities of field identity and field strength. The experimental setup used monoenergetic proton radiography, as illustrated in Fig. 1(a). A pulse of 14.9-MeV protons was generated from fusion reactions of deuterium (D) and helium-3 ($^3$He) in a $D_2$-$^3$He-filled, glass-shell capsule driven by 17 OMEGA [8] laser beams. This proton source was completely characterized using spectral [9], spatial [10], and temporal [11] diagnostics; it had mean energy $14.9 \pm 0.1$ MeV, spectral half-width $<1.5\%$ (or half-width in the proton velocity distribution $<0.75\%$), emission region FWHM $\approx 45$ $\mu$m, and duration $\approx$ 130 ps. The protons were used to image two identical, expanding plasma bubbles, formed on opposite sides of a 5-$\mu$m-thick plastic (CH) foil by two 1-ns-long laser interaction beams. Both beams had spot diameters of 850 $\mu$m and intensities of $8 \times 10^{13}$ W/cm$^2$; they were fired simultaneously and incident at 23.5° from the normal to the foil.

 

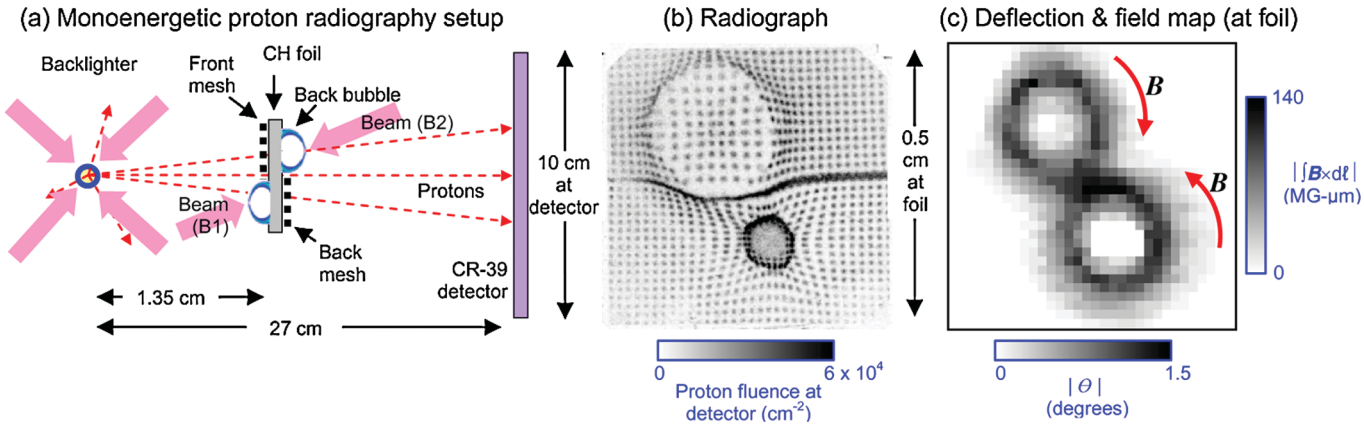


FIG. 1 (color). Proton radiography setup (a), proton radiograph of two laser-generated plasma bubbles (b), and spatial map of proton beamlet deflection angle as a function of position on the foil (c). It will be seen in Fig. 2(b) that the deflections are associated almost exclusively with a $\boldsymbol{B}$ field near the foil, and this means that (c) can also be viewed as a magnetic-field map. Panel (c) shows that the two bubbles were actually the same size even though the apparent sizes are different in the radiograph. The orientation of the images is as seen from behind the detector, looking toward the backlighter. The radiograph was acquired during OMEGA shot 46535.

To break the nearly isotropic proton fluence into "beamlets" (~1000 protons each) whose deflections could easily be observed and quantified, 150-$\mu$m-period nickel meshes were placed on opposite sides of the foil. Figure 1(b) is the resulting radiograph, recorded on a CR-39 nuclear track detector [9], with laser timing adjusted so the bubbles were recorded 1.36 ns after the onset of the interaction beams.

The top bubble image in Fig. 1(b) is a type of image we have recently begun studying [12,13] and contrasting to predictions of the 2D radiation-hydrodynamic code LASNEX [14]. The simulations indicated that proton deflections are purely a result of a toroidal $\boldsymbol{B}$, parallel to the foil, arising from the $\nabla n_e \times \nabla T_e$ magnetic-field source term (where $n_e$ and $T_e$ are the electron number density and temperature) [15,16]. While the data and simulations were qualitatively similar, there was a consistent, quantitative mismatch between them throughout the bubble evolution (predicted apparent bubble sizes were ~25% smaller than observed [17,18]; predicted values of $\int \boldsymbol{B} \times d\ell$ were larger overall than observed; and field morphology details differed). This discrepancy effectively precluded use of the simulations to justify any *a priori* assumption that observed proton deflections were caused exclusively by a $\boldsymbol{B}$ field and not by any component $\boldsymbol{E}_\parallel$ (parallel to the foil) of an $\boldsymbol{E}$ field.

To provide direct experimental identification of the field type as well as strength, the current experiment was designed so the second bubble reverses the sign of any $\boldsymbol{B}$ relative to the first bubble (as seen from the detector) while leaving any $\boldsymbol{E}_\parallel$ unchanged. If the $\boldsymbol{B}$ reversal had no effect on deflections of the monoenergetic protons used to image the plasma, any deflections would necessarily have been dominated by $\boldsymbol{E}_\parallel$. If the reversal resulted in equal but oppositely directed deflections of the monoenergetic protons, that would demonstrate the clear dominance of $\boldsymbol{B}$. Qualitatively, the latter is what we see in the image: the bubble on the back side of the foil (top of image) appears expanded, and the bubble on the front side appears contracted.

Figure 1(c) shows the absolute values of the beamlet deflection angles $\theta$ as a function of position at the foil; $\theta$ is calculated from the apparent displacement of a beamlet in an image relative to where it would be without deflection. The peak $\theta$ occur at the foil on two circles of the same radius, and the amplitudes are the same for both circles. This is seen quantitatively in Fig. 2(a), which shows $\theta$ as a function of radius measured from each bubble's center. Because of Eq. (1), and the fact that $\boldsymbol{B}$ is reversed between the bubbles while $\boldsymbol{E}$ is not, it follows that we can decompose the total deflections $\theta_{\text{top}}(r)$ and $\theta_{\text{bottom}}(r)$ for the top and bottom bubbles into parts due only to $\boldsymbol{B}$ and $\boldsymbol{E}$ by assuming the two bubbles are otherwise equivalent. Then

$$\theta_{\text{top}}(r) = \theta_E(r) + \theta_{B,\text{top}}(r), \tag{2}$$

$$\theta_{\text{bottom}}(r) = \theta_E(r) - \theta_{B,\text{top}}(r), \tag{3}$$

from which it follows that

$$\theta_E(r) = [\theta_{\text{top}}(r) + \theta_{\text{bottom}}(r)]/2, \tag{4}$$

$$\theta_B(r) = [\theta_{\text{top}}(r) - \theta_{\text{bottom}}(r)]/2. \tag{5}$$

The results are shown in Fig. 2(b) after converting $\theta_B(r)$ and $\theta_E(r)$ to $\int \boldsymbol{B} \times d\ell$ and $\int \boldsymbol{E}_\parallel \times d\ell$ using Eq. (1). The vertical display scales for $\boldsymbol{E}$ and $\boldsymbol{B}$ were selected so the relative amplitudes of the curves indicate the relative amounts of proton deflection. The effect of $\boldsymbol{B}$ greatly dominates the effect of $\boldsymbol{E}_\parallel$, whose measured amplitude is smaller than measurement uncertainties [19].

Figure 1(c) reveals a toroidal topology for the $B$ field. An estimate of the maximum local $|\boldsymbol{B}|$ for a toroidal height of 400 $\mu$m (assuming a height of order the shell thickness) is

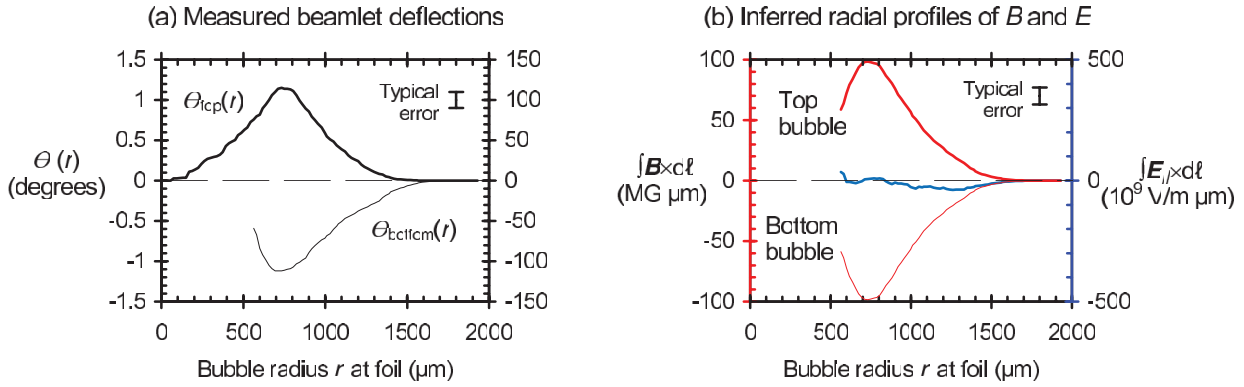


FIG. 2 (color). (a) Measured beamlet deflection angles $\theta$ as a function of radius $r$ in the top and bottom bubbles of Fig. 1(b) (positive is away from the bubble center) and (b) inferred radial profiles of $\int \boldsymbol{B} \times d\ell$ and $\int \boldsymbol{E}_{\parallel} \times d\ell$ in the two bubbles. In (b), the vector $\int \boldsymbol{B} \times d\ell$ is plotted as a positive number for a toroidal $\boldsymbol{B}$ field in the clockwise direction of Fig. 1(c), while $\int \boldsymbol{E}_{\parallel} \times d\ell$ is plotted as positive for an $\boldsymbol{E}$ field pointing away from the bubble center. $\boldsymbol{B}$ has opposite directions in the two bubbles, while $\boldsymbol{E}$ has the same direction. Note that the absence of information about $\theta_{\text{bottom}}$ for $r < \sim 500$ $\mu$m reflects the overlap of beamlets in the center of the bottom bubble image in Fig. 1(b), which prevented beamlet deflection measurements in that region.

then 100 MG $\mu$m/400 $\mu$m $\sim$ 0.3 MG. For this field, the Hall parameter $\omega_{ce}\tau$ (where $\omega_{ce}$ is the electron gyrofrequency and $\tau$ is the electron-ion collision time [15,16]) is of order 1. Since thermal conductivity goes as $1/[1 + (\omega_{ce}\tau)^2]$ (Refs. [15,20]), it follows that field-induced inhibition of thermal transport across the plasma bubble boundary will occur.

Interestingly, this may provide insight as to why the simulations, while correctly predicting that a toroidal $\boldsymbol{B}$ field was the primary cause of the deflections, could overestimate the field and underestimate the bubble size. Thomson scattering [21] measurements recorded at the same time as the Fig. 1(b) radiograph (1.36 ns) indicated that, while the measured electron temperature was well matched by LASNEX simulations at the center of the plasma (450 $\mu$m above the foil), the electron temperature 600 $\mu$m away from the axis was $\sim$40% lower than the predicted value (700 eV) [22]. With the predicted temperature too high in the region of maximum $B$ field, the predicted magnetic diffusivity would be too low (since it is proportional to $T^{-3/2}$ [15]) and the predicted $\boldsymbol{B}$ field would dissipate too slowly, leading to higher field strengths, higher $\omega_{ce}\tau$, and an even more slowly decaying electron temperature. Such considerations and more detailed data and simulation comparisons will be important for advancing our basic understanding and our predictive capabilities with various codes.

The absolute experimental determination here that the fields responsible for the structure of Fig. 1(b) are magnetic allows us to revisit the images of Refs. [12,13] (showing radiographs of similar plasma bubbles on one side of the foil only) with confidence that they also reflect magnetic fields. Reference [12] shows images representing the complete time evolution of bubble structure throughout the 1-ns laser pulse and for an additional 2 ns afterward. Those images were recorded with the same integration time ($\sim$130 ps) as used here, and show the temporal evolution of the plasma bubble radius and field magnitude. In addition, a breakdown in azimuthal symmetry was observed at times slightly later than that of Fig. 1(b) here.

Essential to the successful implementation of the technique of field discrimination and quantification are the isotropic and monoenergetic characteristics of the protons (the velocity uncertainty was $<$1% over the imaged plasma). Other recent important methods of ion generation from intense laser-plasma interactions [23–25], while useful in different radiographic settings, would be compromised in the present context because of the energy spread and anisotropy of the ion fluences. And other techniques of single-point field measurement at extremely high laser intensities ($\sim 10^{20}$ W/cm$^2$, Ref. [26]) do not generate global field maps that show the entire laser-plasma morphology, a prerequisite to understanding plasma dynamics.

Variations of this monoenergetic proton radiography are now being applied to other important plasma or field problems in high-energy-density physics. For example, recent work [6] in inertial confinement fusion [27,28] showed, through single-sided monoenergetic proton radiography, the presence of strong striated fields around an imploding capsule. Unresolved in this work was the issue of whether the striated fields were magnetic or electric. Yet the identification of field type is of paramount importance because different fields would involve different generation mechanisms and would have a significantly different impact on plasma evolution (through such processes as thermal transport modification). By simultaneously irradiating a subject implosion from two different directions, the methodology described above can unambiguously discern whether these fields are magnetic or electric. If magnetic in character, it is quite possible that the striations are a result

of an electrothermal instability [29], potentially leading to the seeding of Rayleigh-Taylor instabilities [29] that could deleteriously impact implosion dynamics [30].

In another experiment involving accelerating rippled plasma foils [31], $\boldsymbol{B}$ fields are suspected—through the mechanism of the Rayleigh-Taylor instability [30]—as the cause of monoenergetic proton deflections seen when the foil was irradiated from a single side [32]. However, unique field and instability identification will probably only be established by irradiating the same foil with monoenergetic protons from the opposite direction as was done in the dual bubble experiment described in this Letter. In general, applications of these field-mapping radiographs to a large class of high-energy-density plasmas will lead to quantifying the nature, the physical extent, and the evolution of embedded, spontaneous fields. By inference, this should also lead to new insights into the origin and dynamics of the pervasive fields of stellar jets [33] and nebulae [34], a major goal of laboratory astrophysics [2,35].

This work was supported by the Fusion Science Center (FSC) at the University of Rochester (Grant No. DE-FG03-03NA00058), the National Laser Users Facility (Grant No. DE-FG52-07NA28059), the Office of Defense Programs (Grant No. DE-FG52-06NA26203), Lawrence Livermore National Laboratory (subcontract Grant No. B5504974), and Laboratory for Laser Energetics at University of Rochester (subcontract Grant No. 412160-001G), all through the U.S. Department of Energy. J. R. R. acknowledges the FSC for additional support. In addition, the authors express their gratitude to General Atomics and the Laboratory for Laser Energetics (LLE) for target fabrication, and to the LLE laser operations team.

*Present address: Lawrence Livermore National Laboratory, Livermore, CA 94551, USA.

[1] W. Baumjohann and R. A. Treumann, *Basic Space Plasma Physics* (Imperial College, London, 1996).
[2] B. Remington *et al.*, Science **284**, 1488 (1999).
[3] E. N. Parker, Astrophys. J. **128**, 664 (1958).
[4] R. P. Drake, *High-Energy-Density Physics* (Springer, New York, 2006).
[5] W. L. Kruer, *The Physics of Laser Plasma Interactions* (Westview, Boulder, CO, 2003).
[6] J. R. Rygg *et al.*, Science **319**, 1223 (2008).
[7] C.K. Li *et al.*, Phys. Rev. Lett. **102**, 205001 (2009).
[8] J. M. Soures *et al.*, Phys. Plasmas **3**, 2108 (1996).
[9] F. H. Seguin *et al.*, Rev. Sci. Instrum. **74**, 975 (2003).
[10] F. H. Seguin *et al.*, Phys. Plasmas **13**, 082704 (2006).
[11] J. A. Frenje *et al.*, Phys. Plasmas **11**, 2798 (2004).
[12] C. K. Li *et al.*, Phys. Rev. Lett. **99**, 015001 (2007).
[13] C. K. Li *et al.*, Phys. Rev. Lett. **99**, 055001 (2007).
[14] G. B. Zimmerman and W. L. Kruer, Comments Plasma Phys. Controlled Fusion **2**, 51 (1975).
[15] S. I. Braginskii, *Review of Plasma Physics 1* (Consultants Bureau, New York, 1965).
[16] M. G. Haines, Phys. Rev. Lett. **47**, 917 (1981).
[17] The disagreement between experiment and LASNEX simulation appeared to be less pronounced than this in an earlier publication [18], but that was because the simulation utilized slightly incorrect imaging system dimensions.
[18] C. K. Li *et al.*, Phys. Rev. Lett. **97**, 135003 (2006).
[19] Measurement of electric fields perpendicular to the foil in a single-bubble experiment was presented in C. K. Li *et al.*, Rev. Sci. Instrum. **77**, 10E725 (2006).
[20] D. S. Montgomery *et al.*, Phys. Rev. Lett. **73**, 2055 (1994).
[21] D. H. Froula *et al.*, Rev. Sci. Instrum. **77**, 10E522 (2006).
[22] On the bubble axis at 1000 $\mu$m above the foil, the measured temperature at 1.36 ns was also ~40% smaller than the LASNEX prediction. Together with the similar result at 600 $\mu$m off axis, this could indicate that plasma cooling effects near the bubble edge are larger than LASNEX predictions when the laser is off, leading to a reduced plasma temperature.
[23] B. M. Heglich *et al.*, Nature (London) **439**, 441 (2006).
[24] M. Borghesi *et al.*, Phys. Rev. Lett. **81**, 112 (1998).
[25] A. J. Mackinnon *et al.*, Phys. Rev. Lett. **97**, 045001 (2006).
[26] M. Tatakaris *et al.*, Nature (London) **415**, 280 (2002).
[27] J. Nuckolls *et al.*, Nature (London) **239**, 139 (1972).
[28] S. Atzeni and J. Meyer-Ter-Vehn, *The Physics of Inertial Fusion* (Oxford University, Oxford, 2004).
[29] M. G. Haines, Can. J. Phys. **64**, 912 (1986).
[30] A. Nishiguchi, Jpn. J. Appl. Phys. **41**, 326 (2002).
[31] V. A. Smalyuk *et al.*, Phys. Rev. Lett. **101**, 025002 (2008).
[32] R. D. Petrasso *et al.*, Bull. Am. Phys. Soc. **52**, 97 (2007).
[33] P. Hartigan *et al.*, arXiv:astro-ph/0702174.
[34] J. J. Hester *et al.*, Astrophys. J. **456**, 225 (1996).
[35] D. D. Ruytov *et al.*, Phys. Plasmas **8**, 1804 (2001).